Available online at www.sciencedirect.com
SCIENCE DIRECT®
Wave Motion 38 (2003) 189–206
WAVE MOTION
www.elsevier.com/locate/wavemoti

Numerical methods for locating small dielectric inhomogeneities

Darko Volkov

Department of Mathematical Sciences, New Jersey Institute of Technology, 606 Cullimore Hall, University Heights, Newark, NJ 07102, USA

Received 3 February 2003; received in revised form 14 February 2003; accepted 26 February 2003

Abstract

We present numerical simulations illustrating the reconstruction of data for electromagnetic inverse problems. Two situations are considered: prescribed electric field and measured magnetic field at the boundary of a medium with cylindrical symmetries, and the analysis of the far field pattern of a scattered field produced by the incidence of an incoming wave on a set of small inhomogeneities.

1. Introduction

Dielectric inhomogeneities of small diameter cause a perturbation of the ambient electromagnetic fields. It is easily conceivable that measuring those perturbations could provide information relevant to the identification and characterization of the inhomogeneities. Engineers have been using that idea for a long time, see [8]. That technique was also applied to medical imaging via magnetic resonance. Recently, a mathematical theory was developed to quantify the perturbation of electromagnetic fields due to inhomogeneities. In the case of a medium whose boundary can be subjected to a time sinusoidal electric field, asymptotic expansions of the perturbed magnetic field, in the relative diameter of the imperfections, were derived in [3,4,7,18]. It was claimed that those asymptotic formulas could be used for solving the inverse problem consisting of reconstructing the imperfections based on measurements of perturbed fields. Some numerical simulations, as in [2], were conducted in an effort to demonstrate the efficiency of the reconstruction algorithm. However, those simulations were based on synthetic data that did not take into account higher errors in the asymptotic approximation induced by working with high frequencies or highly oscillatory currents in amplitude versus space variables. We propose to discuss in this paper these hurdles and we show on a numerical simulation how they can be overcome. Note that in this paper, unlike in [2], the numerical data is actually coming from solving the time harmonic wave equation using a highly accurate numerical scheme. Therefore, we believe that our numerical data follows closely what would be measured in a real life situation provided that the required boundary fields could be accurately generated.

In the mathematical study of the perturbed field, asymptotic formulas were also derived for the far field pattern of the scattered wave produced by an incoming wave impinging a set of inhomogeneities, see [1,5,6]. The possible applications that we bear in mind in this context range from radar imaging to the detection of mines. In [13] the authors solve an inverse problem for perfectly conducting inhomogeneities from scattered field data. In [1] the possibility of devising a reconstruction of dielectric inhomogeneities algorithm from data measured at a single

E-mail address: darko.volkov@njit.edu (D. Volkov).

0165-2125/$ – see front matter © 2003 Elsevier Science B.V. All rights reserved.
doi:10.1016/S0165-2125(03)00047-7

frequency but from different observation and incidence angles, is considered. In this paper a different algorithm is proposed and is tested on simulated data. This algorithm is based on projections on three different planes. In terms of computational time this method amounts to solving three times a two-dimensional problem. This is a great saving as compared to a full fledged three-dimensional approach making use of spherical harmonics.

2. Identifying inhomogeneities using prescribed fields on the boundary

In this section we are interested in an inverse problem for the two-dimensional Helmholtz equation in a bounded domain Ω. It is well known in the literature that they can be viewed as the reduced time harmonic Maxwell's equations for the case of cylindrical symmetries. We chose to look at TE (transverse electric) symmetries. Imposing an alternating current at the boundary of the domain amounts to setting Dirichlet data for the Helmholtz problem. We denote ν the outward unit normal to $\partial\Omega$. We assume that Ω contains a finite number of inhomogeneities, each of the form $z_j + \alpha B_j$, where $B_j \subset \mathbf{R}^2$ is a bounded, smooth domain containing the origin. The total collection of inhomogeneities is

$$\mathcal{B}_\alpha = \bigcup_{j=1}^{m} \{z_j + \alpha B_j\}.$$

The points $z_j \in \Omega$, $j = 1, \ldots, m$, which determine the location of the inhomogeneities, are assumed to satisfy the following inequalities:

$$|z_j - z_l| \geq c_0 > 0 \quad \forall j \neq l \quad \text{and} \quad \operatorname{dist}(z_j, \partial\Omega) \geq c_0 > 0 \quad \forall j. \tag{1}$$

Assume that $\alpha > 0$, the common order of magnitude of the diameters of the inhomogeneities, is sufficiently small, that these inhomogeneities are disjoint, and that their distance to $\mathbf{R}^2 \setminus \bar{\Omega}$ is larger than $c_0/2$. Let μ_0 and ε_0 denote the permeability and the permittivity of the background medium. Let them satisfy the usual requirements $\mu_0 > 0$ and $\operatorname{Re}\varepsilon_0 > 0$, $\operatorname{Im}\varepsilon_0 \geq 0$. Let $\mu_j > 0$ and $\operatorname{Re}\varepsilon_j > 0$, $\operatorname{Im}\varepsilon_j \geq 0$ denote the permeability and the permittivity of the jth inhomogeneity, $z_j + \alpha B_j$. Introduce the piecewise constant magnetic permeability

$$\mu_\alpha(x) = \begin{cases} \mu_0, & x \in \Omega \setminus \bar{\mathcal{B}}_\alpha, \\ \mu_j, & x \in z_j + \alpha B_j, \quad j = 1, \ldots, m. \end{cases} \tag{2}$$

If we allow the degenerate case $\alpha = 0$, then the function $\mu_0(x)$ equals the constant μ_0. The piecewise constant electric permittivity, $\varepsilon_\alpha(x)$ is defined analogously. Consider the solutions to the time harmonic Maxwell's equations with TE symmetry and $\exp(-\mathrm{i}\omega t)$ time dependence. Let E_α be the electric field (or rather, the transverse strength) in the presence of the inhomogeneities. It satisfies the Helmholtz equation

$$\operatorname{div}\left(\frac{1}{\mu_\alpha}\operatorname{grad} E_\alpha\right) + \omega^2 \varepsilon_\alpha E_\alpha = 0 \quad \text{in } \Omega \tag{3}$$

with the boundary condition $E_\alpha = f$ on $\partial\Omega$, where $\omega > 0$ is a given frequency. We are actually interested in measuring the quantity $(\partial E_\alpha/\partial\nu)|_{\partial\Omega}$. In the cylindrical symmetry model, that quantity is related to the intensity of the tangential magnetic field on Ω. The basic idea relies upon utilizing the prescribed quantity $E_\alpha|_{\partial\Omega}$ and the measured quantity $(\partial E_\alpha/\partial\nu)|_{\partial\Omega}$. Together they make Eq. (3) overdetermined, so they should provide information on the coefficients of that equation.

The electric field, E_0, in the absence of any inhomogeneities, satisfies the following equation:

$$\Delta E_0 + k^2 E_0 = 0 \quad \text{in } \Omega, \tag{4}$$

where $k^2 = \omega^2\mu_0\varepsilon_0$, with $E_0 = f$ on $\partial\Omega$. In order to insure well posedness we shall assume that k^2 is not an eigenvalue for the operator with homogeneous Dirichlet boundary conditions. Under this assumption it was proved

in [18] that Eq. (3) together with the boundary condition $E_\alpha = f$ on $\partial\Omega$ is a well posed problem for α small enough. As α approaches 0, E_α approaches E_0. It is possible to write down an asymptotic expansion for the difference $E_\alpha - E_0$. Such expansions have been derived using rigorous analysis, see [18]. They have also been derived using matched asymptotics, see [2]. These formulas have been verified numerically and used to address the problem of locating and characterizing inhomogeneities. Let v be any function satisfying $(\Delta + k^2)v = 0$ in Ω. The following formula, derived in [2], is an immediate consequence of the asymptotic expansion for the difference $E_\alpha - E_0$

$$\int_{\partial\Omega} \frac{\partial E_\alpha}{\partial \nu} v \, \mathrm{d}\sigma - \int_{\partial\Omega} \frac{\partial v}{\partial \nu} E_\alpha \, \mathrm{d}\sigma = \alpha^2 \sum_{j=1}^{m} \left[\omega^2 \mu_0 (\epsilon_0 - \epsilon_j) |B_j| E_0(z_j) v(z_j) + \left(\frac{\mu_0}{\mu_j} - 1 \right) \mathbf{M}\left(\frac{\mu_j}{\mu_0} \right) \nabla E_0(z_j) \cdot \nabla v(z_j) \right] + \mathrm{O}(\alpha^3). \tag{5}$$

The remainder in the asymptotic formula (5) depends on the constant in (1) but does not otherwise depend on the location of the z_j's. The term $\mathbf{M}(\mu_j/\mu_0)$ is a 2×2 matrix called polarization tensor for the shape B_j. We refer to [10,18] on that subject, although the polarization tensors were first introduced by Schiffer, Pólya, and Szegö, see [14,16,17]. In our numerical experiments $\partial\Omega$ is the unit circle centered at the origin and the shapes B_j are ellipses. The remainder in (5) is then $\mathrm{O}(\alpha^4)$, see [6]. Let ξ be any vector in $\mathbf{R}^2$, $\xi^\perp$ a unit vector orthogonal to ξ and γ a complex number. The function

$$x \to \exp(\mathrm{i}x \cdot (\xi + \gamma \xi^\perp))$$

satisfies the Helmholtz equation in $\mathbf{R}^2$ if and only if γ is a square root of $k^2 - \|\xi\|^2$. Now set for the boundary condition

$$E_\alpha(x) = \exp(\mathrm{i}x \cdot (\xi + \gamma \xi^\perp)), \tag{6}$$

where γ is a fixed square root of $k^2 - \|\xi\|^2$, and

$$v(x) = \exp(\mathrm{i}x \cdot (\xi - \gamma \xi^\perp)). \tag{7}$$

We specialize formula (5) for that choice of E_α and v to obtain

$$\int_{\partial\Omega} \frac{\partial E_\alpha}{\partial \nu} v \, \mathrm{d}\sigma - \int_{\partial\Omega} \frac{\partial v}{\partial \nu} E_\alpha \, \mathrm{d}\sigma = \alpha^2 \sum_{j=1}^{m} \exp(2\mathrm{i}z_j \cdot \xi) \left[\omega^2 \mu_0 (\epsilon_0 - \epsilon_j) |B_j| E_0(z_j) v(z_j) - \left(\frac{\mu_0}{\mu_j} - 1 \right) \mathbf{M}\left(\frac{\mu_j}{\mu_0} \right) (\xi + \gamma \xi^\perp) \cdot (\xi - \gamma \xi^\perp) \right] + \mathrm{O}(\alpha^4). \tag{8}$$

If the matrices $\mathbf{M}(\mu_j/\mu_0)$ are of the form $\mathbf{m}(\mu_j/\mu_0) I_2$, where $\mathbf{m}(\mu_j/\mu_0)$ is a scalar and I_2 is the 2×2 identity (which is satisfied if all shapes are circles see [10] or [19]), then (8) reduces to

$$\int_{\partial\Omega} \frac{\partial E_\alpha}{\partial \nu} v \, \mathrm{d}\sigma - \int_{\partial\Omega} \frac{\partial v}{\partial \nu} E_\alpha \, \mathrm{d}\sigma = \alpha^2 \sum_{j=1}^{m} \exp(2\mathrm{i}z_j \cdot \xi) \left[\omega^2 \mu_0 (\epsilon_0 - \epsilon_j) |B_j| E_0(z_j) v(z_j) - \left(\frac{\mu_0}{\mu_j} - 1 \right) \mathbf{m}\left(\frac{\mu_j}{\mu_0} \right) (2\|\xi\|^2 - k^2) \right] + \mathrm{O}(\alpha^4). \tag{9}$$

In this case since $\|\xi\|^2$ is a polynomial in the coordinates of ξ, the expression in (9) the Fourier transform of a linear combination of derivatives of order less than or equal to 2 of Dirac measures centered at the points $2z_j$ for $1 \le j \le m$. Therefore, a numerical Fourier inversion of a sample of those measurements should efficiently pin

down the z_j's. This approach has been successfully used for the Laplace operator in the context of the conductivity problem, see [2]. However, in the numerical simulations presented by the authors, the starting point was the algebraic expression in the right-hand side of (9). Random noise was added to compensate for the absence of the remainder term. Although if some of the ∂B_j are not circles the expression

$$\sum_{j=1}^{m} \exp(2\mathrm{i} z_j \cdot \xi) \left[\omega^2 \mu_0 (\epsilon_0 - \epsilon_j) |B_j| E_0(z_j) v(z_j) - \left(\frac{\mu_0}{\mu_j} - 1 \right) \mathbf{M} \left(\frac{\mu_j}{\mu_0} \right) (\xi + \gamma \xi^{\perp}) \cdot (\xi - \gamma \xi^{\perp}) \right] \tag{10}$$

is the Fourier transform of an operator of a more complicated kind acting on a linear combination of Dirac measures centered at the points $2z_j$ for $1 \le j \le m$, numerical experiments indicate that a Fourier inversion for retrieving the z_j's works just as well in this case.

In our approach, we chose to simulate the data $\partial E_\alpha / \partial \nu$ using a solver for Eq. (3). Instead of using a generic solver, we wrote a code based on solving singular boundary integral equations on the contours $\partial\Omega$ and ∂B_j, $j = 1, \ldots, m$. Using 64 points on each contour, this numerical method is highly accurate for k, μ_α, ϵ_α in a given range, see [12,19]. We think that this is a more realistic way of simulating noise because in a physical set up the integral on the left-hand side of (8) containing $\partial E_\alpha / \partial \nu$ has to be evaluated from measured data. Let us first review the fundamental mechanism behind the FFT method for inverting the quantity in (10). We think that this review is necessary because it is not obvious how to relate the continuous Fourier transform of a function that does not decrease rapidly, to its discrete FFT. That review will give some insight on how to set numerical values for the range of ξ and how to pick a step size.

2.1. Principle of the FFT method

We have to assume that all the (z_j^1, z_j^2), $j = 1, \ldots, m$, lie in a square $[-a, a] \times [-a, a]$, where a is a known positive number. To make the argument clearer we study the case where the quantity (8) is simply

$$\sum_{j=1}^{m} C_j \, \mathrm{e}^{2\mathrm{i}(\xi_1 z_j^1 + \xi_2 z_j^2)}, \tag{11}$$

where the C_j are some unknown complex constants. We suppose that the quantity (11) is known for ξ in the square $[-\xi_{\max}, \xi_{\max}] \times [-\xi_{\max}, \xi_{\max}]$ on a regular grid made up of n^2 points. So our data is

$$\sum_{j=1}^{m} C_j \exp(2\mathrm{i}(z_j^1(-\xi_{\max} + (j_1 - 1)h) + z_j^2(-\xi_{\max} + (j_2 - 1)h))), \quad 1 \le j_1, \quad j_2 \le n, \tag{12}$$

where $h = 2\xi_{\max}/n$. The inverse FFT applied to our data yields

$$\frac{1}{n^2} \sum_{j=1}^{m} C_j \sum_{j_1, j_2 = 1}^{n} \exp(2\mathrm{i}(z_j^1(-\xi_{\max} + (j_1 - 1)h) + z_j^2(-\xi_{\max} + (j_2 - 1)h))) \times \exp\left(2\mathrm{i}\pi \left(\frac{j_1 - 1}{n}(l_1 - 1) + \frac{j_2 - 1}{n}(l_2 - 1) \right) \right) \tag{13}$$

for $1 \le l_1, l_2 \le n$. An elementary calculation shows that the norm of expression (13) is equal to

$$\left| \sum_{j=1}^{m} C_j \frac{1}{n^2} \frac{\sin(2\xi_{\max} z_j^1) \sin(2\xi_{\max} z_j^2)}{\sin[\pi(z_j^1 h/\pi + (l_1 - 1)/n)] \sin[\pi(z_j^2 h/\pi + (l_2 - 1)/n)]} \right|. \tag{14}$$

As n grows large the above quantity is small unless $(z_j^1 h/\pi + (l_1 - 1)/n)$ and $(z_j^2 h/\pi + (l_2 - 1)/n)$ are each close to an integer. Therefore we choose h such that

$$ah \simeq 1. \tag{15}$$

That way $(z_j^1 h/\pi + (l_1 - 1)/n)$ and $(z_j^2 h/\pi + (l_2 - 1)/n)$ can only approach the integers 0 or 1. $\xi_{\max}$ and n are related by the relation $\xi_{\max}/n = h/2$. The (z_j^1, z_j^2) are located where the norm of (13) peaks. The accuracy of this method is at best $\pi/(2\xi_{\max})$. This accuracy is to be compared to the length of an edge of the square of interest, $2a$, leading to a relative error of $\pi/(4\xi_{\max} a)$ for the location of the centers z_j. Numerical experiments indicate that this accuracy is actually achieved.

2.2. A numerical example

Care must be taken when numerically implementing the method described above. For example, as ξ grows large, γ has a non-zero imaginary part and the functions (6) and (7) become exponentially small or large. The numerical algorithm is then bound to fail as it will attempt to sum numbers of very different magnitudes. One might think that choosing high frequencies, that is a high value for k, would overcome that difficulty. But then the functions (6) and (7) become highly oscillatory which is also a problem. In our numerical example we set the number of inhomogeneities to be equal to 3 (that number is of course an unknown for the inverse problem). The three inhomogeneities are shaped as ellipses characterized by their center, the length of the principal axis a, the length of the smaller axis b, and the angle θ of the principal axis to the x-axis. We chose the numerical data displayed in the following table:

	Background	B_1	B_2	B_3
k	4.0	$4.5 + 2\mathrm{i}$	7.4	0.6
μ	0.5	0.725	0.8	1.2
Center		$(0.31, -0.72)$	$(0.0, -0.12)$	$(-0.43, 0.67)$
a		0.05	0.04	0.035
b		0.03	0.03	0.025
θ		1.0	0.0	-0.5

The domain Ω together with the inhomogeneities have been plotted in Fig. 1.1.

To solve the inverse problem, our basic assumption is that the inhomogeneities lie in the square $[-1, 1]^2$. Then, according to (15) we pick $h = 1$. We pick $\xi_{\max} = 10$ and according to the preceding section we expect a $\pi/(2\xi_{\max}) \simeq 0.16$ order of resolution. However, this approach lead to disastrous results. Indeed, values of ξ as high as $(-10, 10)$ produced functions of very high norm for (6) and (7) for x in Ω as compared to their norm for ξ near 0. We also observed that for high values of $|\xi|$ the $O(\alpha^4)$ remainder in (8) grew very large as compared to the magnitude of (10) for small values of $|\xi|$. When $\xi_{\max}$ is fixed, setting high values for the background k by invoking the possibility of increasing the frequency, makes the parameter γ real for ξ in $[-\xi_{\max}, \xi_{\max}]^2$. But once again the remainder term $O(\alpha^4)$ in (8) grew too large and we were not able to find a good estimate for the expression (10).

To circumvent this difficulty our idea was then to pick a threshold ξ_0 such that for $\|\xi\| > \xi_0$ we set the quantity in (10) to be equal to 0. To compensate for the loss of accuracy due to this cut off we choose a much finer grid. That way we were able to keep the remainder in (8) reasonably small. The value of the cut off ξ_0 and the step size for the grid were obtained through numerical simulations. These numbers depend on k, on the relative size of the inhomogeneities, α, on the distance c defined in (1), on bounds for the values of k and μ inside the inhomogeneities but is otherwise independent of the locations z_j, the shapes B_j and the values of k and μ inside the inhomogeneities.

To get a feel of how the cut off method works, we re-examine the model quantity (12) from the last section. The cut off method amounts to knowing the value of quantity (12) only for $(n/2) - p \le j_1, j_2 \le (n/2) + p - 1$ for some integer p less than $n/2$. The inverse FFT applied to our data yields

$$\frac{1}{n^2}\sum_{j=1}^{m} C_j \sum_{j_1, j_2 = (n/2)-p}^{(n/2)+p-1} \exp(2\mathrm{i}(z_j^1(-\xi_{\max} + (j_1 - 1)h) + z_j^2(-\xi_{\max} + (j_2 - 1)h))) \times \exp\left(2\mathrm{i}\pi\left(\frac{j_1 - 1}{n}(l_1 - 1) + \frac{j_2 - 1}{n}(l_2 - 1)\right)\right) \tag{16}$$

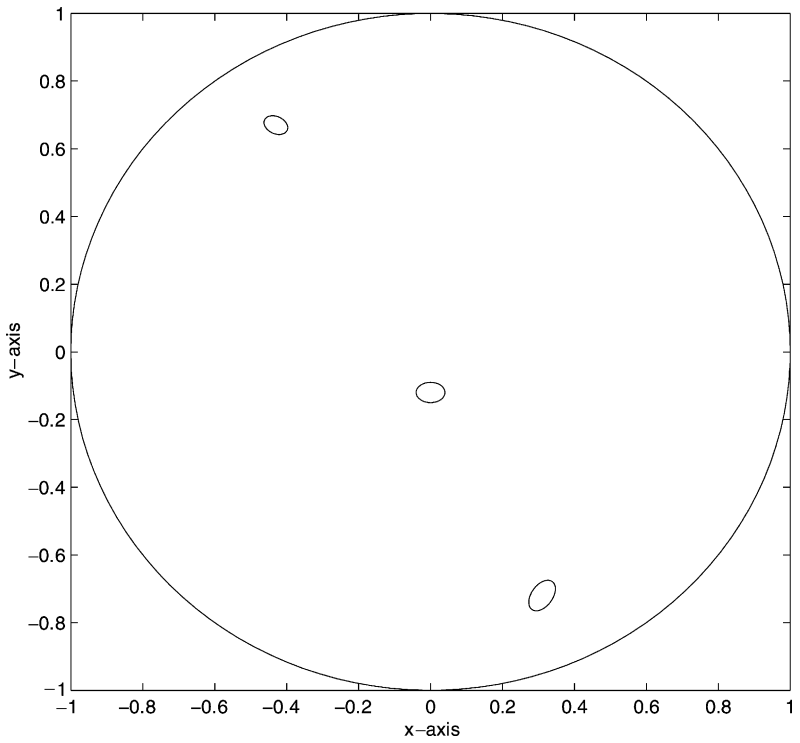

Fig. 1.1. The three inhomogeneities inside the domain Ω.

for $1 \le l_1, l_2 \le n$. An elementary calculation shows that the norm of expression (13) is equal to

$$\left| \sum_{j=1}^{m} C_j \frac{1}{n^2} \frac{\sin\left[2p(hz_j^1 + \pi(l_1 - 1)/n)\right] \sin\left[2p(hz_j^2 + \pi(l_2 - 1)/n)\right]}{\sin\left[\pi(z_j^1 h/\pi + (l_1 - 1)/n)\right] \sin\left[\pi(z_j^2 h/\pi + (l_2 - 1)/n)\right]} \right|. \tag{17}$$

If, for a fixed j, $(z_j^1 h/\pi + (l_1 - 1)/n)$ and $(z_j^2 h/\pi + (l_2 - 1)/n)$ are each close to an integer then the quantity (17) is roughly of the order of $|C_j(4p^2/n^2)|$. If for each $j(z_j^1 h/\pi + (l_1 - 1)/n)$ and $(z_j^2 h/\pi + (l_2 - 1)/n)$ are not close to an integer then quantity (17) is much smaller.

We now present a successful case where the ratio n/p is chosen to be close to 5. We set $\xi_{\max} = 13$ for the dimension of the Fourier domain, $\xi_0 = \|(2.5, 2.5)\|$ for the cut off and place 260×260 points on a regular grid in $[-\xi_{\max}, \xi_{\max}]^2$. Then we run our code to solve Eq. (3) with Dirichlet data (6). Next we computed (10) using the trapezoidal rule and we stored the result in a file. We then apply to that data the inverse FFT routine. We obtain a result in the x, y coordinates in the square $[-130/2\pi\xi_{\max}, 130/2\pi\xi_{\max}]^2$, where $130/2\pi\xi_{\max} \simeq 15.7$ and an expected accuracy of $\pi/2\xi_{\max} \simeq 0.12$. We represent on a three-dimensional plot in Fig. 1.2 the norm of the result in the square of interest, that is the square $[-1, 1]^2$. The same result is plotted using contour maps in Fig. 1.3. Equally satisfactory reconstruction were obtained for different values of the centers z_j. It is, however, worth reporting that if one of the inhomogeneities has a value of k that contrasts with the value of the background k in a much larger scale as compared to the other inhomogeneities, then only the inhomogeneity with the sharpest contrast will appear in the reconstructed image.

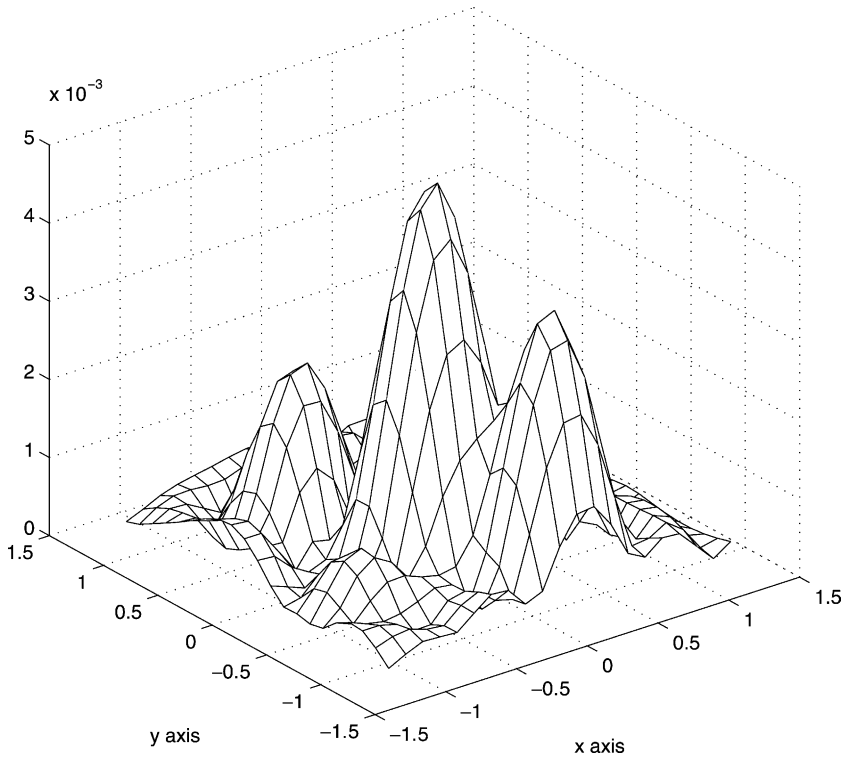

Fig. 1.2. Reconstruction of the inhomogeneities in Ω.

3. Reconstruction of inhomogeneities from the far field pattern at a fixed frequency

In this section we consider the scattering problem for the full Maxwell's equations from a collection of dielectric inhomogeneities of small diameter. We suppose that there is a finite number of dielectric imperfections in $\mathbf{R}^3$, each of the form $z_j + \alpha B_j$, where $B_j \subset \mathbf{R}^3$ is a bounded, domain containing the origin. We preserve the same notations as in the preceding section for the inhomogeneities B_j and the functions μ_α and ϵ_α. The only modification is to set $\Omega = \mathbf{R}^3$.

We need this time to give the precise definition of polarization tensors. Let γ^j, $1 \le j \le m$, be a set of positive constants or complex constants whose real and imaginary parts are positive. In effect, $\{\gamma^j\}$ will be either the set $\{\epsilon^j\}$ or the set $\{\mu^j\}$. For any fixed $1 \le j_0 \le m$, let γ denote the coefficient given by

$$\gamma(x) = \begin{cases} \gamma^0, & x \in \mathbf{R}^3 \setminus \overline{B_{j_0}}, \\ \gamma^{j_0}, & x \in B_{j_0}. \end{cases} \tag{18}$$

By ϕ_l, $1 \le l \le 3$, we denote the solution to

$$\nabla_y \cdot \gamma(y) \nabla_y \phi_l = 0 \quad \text{in } \mathbf{R}^3, \qquad \phi_l - y_l \to 0 \quad \text{as } |y| \to \infty.$$

This problem may alternatively be written as

$$\Delta \phi_l = 0 \quad \text{in } B_{j_0} \text{ and in } \mathbf{R}^3 \setminus \overline{B_{j_0}}, \qquad \phi_l \text{ is continuous across } \partial B_{j_0},$$
$$\frac{\gamma^0}{\gamma^{j_0}} (\partial_\nu \phi_l)^+ - (\partial_\nu \phi_l)^- = 0 \quad \text{on } \partial B_{j_0}, \qquad \phi_l(y) - y_l \to 0 \quad \text{as } |y| \to \infty.$$

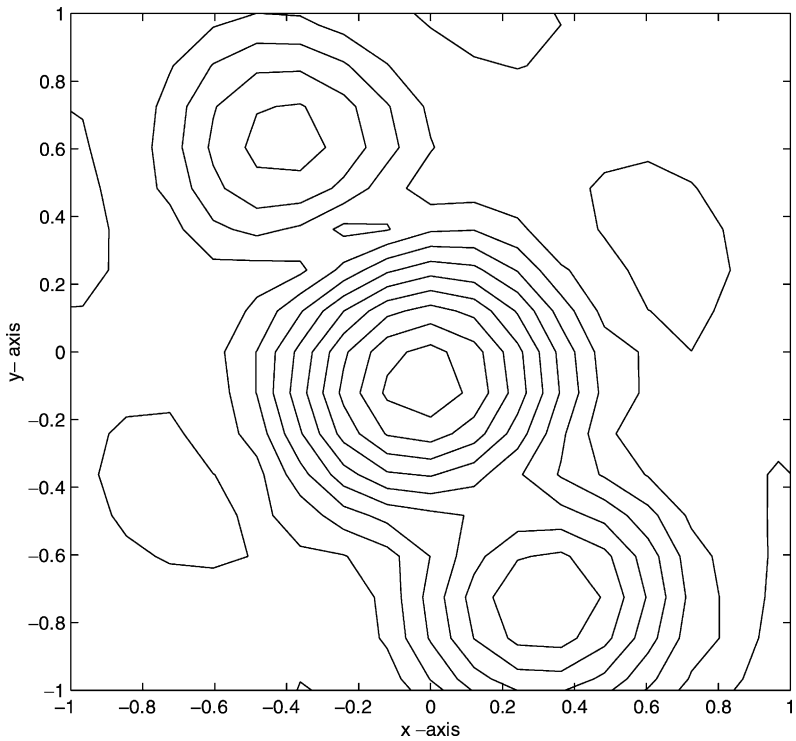

Fig. 1.3. Reconstruction of the inhomogeneities in Ω: contour map.

Here ν denotes the outward unit normal to $\partial(B_{j_0})$; superscript $+$ and $-$ indicate the limiting values as we approach $\partial(B_{j_0})$ from outside B_{j_0}, and from inside B_{j_0}. It is obvious that the function ϕ_l only depends on the coefficients γ^0 and γ^{j_0} through the ratio $c = \gamma^0/\gamma^{j_0}$. The existence and uniqueness of this ϕ_l can be established using single layer potentials with suitably chosen densities. It is essential here, that the constant c, by assumption, cannot be 0 or a negative real number. We now define the polarization tensor, $M^{j_0}(c)$ of the inhomogeneity B_{j_0} (with aspect ratio c) by

$$M_{kl}^{j_0}(c) = c^{-1} \int_{B_{j_0}} \partial_{y_k} \phi_l \, \mathrm{d}y. \tag{19}$$

It can be seen that the tensor $M_{kl}^{j_0}(c)$ is symmetric; if c is a positive real number, it is furthermore positive definite, see [10,11]. For the analogous problem in $\mathbf{R}^2$, it is well known that the polarization tensor defined above is a multiple of the identity. An exact formula for the value of this multiple is known. For the problem in $\mathbf{R}^3$ a similar statement can be derived.

Lemma 3.1. *Suppose B_{j_0} is a sphere. Then the matrix $M_{kl}^{j_0}(c)$ defined in (19) is a multiple of the identity matrix. That multiple is*

$$2|B_{j_0}| \frac{\gamma^{j_0}}{\gamma_0} \frac{\gamma^{j_0} - \gamma_0}{2\gamma^{j_0} + \gamma_0}. \tag{20}$$

Proof. Without loss of generality we can assume that B_{j_0} is a sphere centered at 0. For that particular geometry, we can find a closed form solution to (19). Without loss of generality we assume that ∂B_{j_0} is centered at 0 and we

denote R its radius. The function $\psi_l = \phi_l - y_l$ satisfies

$$\Delta\psi_l = 0 \quad \text{in } B_{j_0} \text{ and in } \mathbf{R}^3 \setminus \overline{B_{j_0}}, \qquad \psi_l \text{ is continuous across } \partial B_{j_0},$$
$$\frac{\gamma^0}{\gamma^{j_0}}(\partial_\nu \psi_l)^+ - (\partial_\nu \psi_l)^- = \left(\frac{\gamma^0}{\gamma^{j_0}} - 1\right)\nu_l \quad \text{on } \partial B_{j_0}, \qquad \psi_l(y) \to 0 \quad \text{as } |y| \to \infty.$$

It is natural to seek ψ_l as an infinite sum of bounded spherical harmonics in B_{j_0} and $\mathbf{R}^3 \setminus \overline{B_{j_0}}$. The reader can consult [15] on the subject of harmonic functions inside and outside a sphere. It turns out that only one term is not zero and we find

$$\psi_l(y) = \begin{cases} \dfrac{\gamma^{j_0} - \gamma_0}{2\gamma^{j_0} + \gamma_0} y_l & \text{in } B_{j_0}, \\ \dfrac{\gamma^{j_0} - \gamma_0}{2\gamma^{j_0} + \gamma_0} y_l \dfrac{R^3}{|y|^3} & \text{in } \mathbf{R}^3 \setminus \overline{B_{j_0}}. \end{cases} \tag{21}$$

Consequently,

$$M_{kl}^{j_0}\left(\frac{\gamma_0}{\gamma^{j_0}}\right) = \frac{\gamma^{j_0}}{\gamma_0}\int_{B_{j_0}} \partial_{y_k}(\psi_l + y_l) = \delta_{kl} 2|B_{j_0}|\frac{\gamma^{j_0}}{\gamma_0}\frac{\gamma^{j_0} - \gamma_0}{2\gamma^{j_0} + \gamma_0}. \qquad \square$$

Define an incident electric plane wave E_0 by

$$E_0(x) = \nabla \times (\mathrm{e}^{\mathrm{i}k\eta\cdot x}\lambda), \tag{22}$$

where η is a vector on the unit sphere S^2 in $\mathbf{R}^3$, λ is any vector in $\mathbf{R}^3$, and $k = \omega\sqrt{\epsilon^0\mu^0}$. E_0 satisfies

$$\left(\nabla \times \frac{1}{\mu^0}\nabla \times -\omega^2\epsilon^0\right) E_0 = 0 \quad \text{in } \mathbf{R}^3. \tag{23}$$

In the presence of inhomogeneities the total field E_α satisfies

$$\left(\nabla \times \frac{1}{\mu_\alpha}\nabla \times -\omega^2\epsilon_\alpha\right) E_\alpha = 0 \quad \text{in } \mathbf{R}^3 \tag{24}$$

with the outgoing radiation condition as $|x| \to \infty$

$$\left|\sqrt{\epsilon^0}(E_\alpha - E_0) - \frac{1}{\mathrm{i}\omega\sqrt{\mu^0}}(\nabla \times (E_\alpha - E_0)) \times \frac{x}{|x|}\right| = \mathrm{O}\left(\frac{1}{|x|^2}\right). \tag{25}$$

It is well known in the literature, see for example [9] or [15], that there exists a unique weak solution to (24) and (25).

The scattering amplitude, $A_\alpha(x/|x|, \eta, \lambda, k)$, is of particular interest. It is defined as

$$E_\alpha(x) = E_0(x) + A_\alpha\left(\frac{x}{|x|}, \eta, \lambda, k\right)\frac{\mathrm{e}^{\mathrm{i}k|x|}}{|x|} + \mathrm{O}\left(\frac{1}{|x|^2}\right) \tag{26}$$

as $|x| \to \infty$. In [5] the following asymptotic formula for the scattering amplitude was derived:

$$A_\alpha\left(\frac{x}{|x|}, \eta, \lambda, k\right) = \frac{-\mathrm{i}k^3}{4\pi}\alpha^3 \sum_{j=1}^{m}\left[\left(\frac{\mu^0}{\mu^j} - 1\right)\left(M^j\left(\frac{\mu^0}{\mu^j}\right)(\eta \times (\eta \times \lambda))\right)\right.$$
$$\left. \times \frac{x}{|x|} + \left(\frac{\epsilon^0}{\epsilon^j} - 1\right)\left(I_3 - \frac{x}{|x|}\frac{x}{|x|}^t\right) M^j\left(\frac{\epsilon^0}{\epsilon^j}\right)(\eta \times \lambda)\right] \mathrm{e}^{\mathrm{i}k(\eta - x/|x|)\cdot z_j} + \mathrm{O}(\alpha^4). \tag{27}$$

A different approach was adopted in [1]. Instead of considering the full 3D Maxwell's equations, the authors were interested in the piecewise Helmholtz equation for a scalar function u_α with the appropriate decay condition at infinity and the required continuity of u_α and $\mu_\alpha(\partial u_\alpha/\partial \nu)$ across the boundaries B_j. The final formula for the scattering amplitude was found in [1] to be

$$A_\alpha\left(\frac{x}{|x|},\eta,k\right)=\frac{k^2}{4\pi}\alpha^3\sum_{j=1}^{m}\mathrm{e}^{\mathrm{i}k(\eta-x/|x|)\cdot z_j}\left[\left(\frac{\mu^j}{\mu^0}-1\right)\frac{x}{|x|}\cdot\left(M^j\left(\frac{\mu^0}{\mu^j}\right)\eta\right)-\left(\frac{\epsilon^0}{\epsilon^j}-1\right)|B_j|\right]+\mathrm{O}(\alpha^4). \tag{28}$$

We now attempt to relate formulas (27) and (28). We assume that all the inhomogeneities B_j are spheres. Thus we can set $M^j(\mu^0/\mu^j)=\mathbf{m}^j(\mu^0/\mu^j)I_3$ and $M^j(\epsilon^0/\epsilon^j)=\mathbf{m}^j(\epsilon^0/\epsilon^j)I_3$. We first examine the case where $x/|x|$ and η are not parallel. In formula (27) we pick $\lambda=x/|x|$. We notice that

$$\frac{x^t}{|x|}\left(\eta\times\frac{x}{|x|}\right)=0$$

and

$$\left(\eta\times\left(\eta\times\frac{x}{|x|}\right)\right)\times\frac{x}{|x|}=\left(\eta\cdot\frac{x}{|x|}\right)\eta\times\frac{x}{|x|}$$

and rewrite (28) as

$$A_\alpha\left(\frac{x}{|x|},\frac{x}{|x|},\eta,k\right)=\frac{-\mathrm{i}k^3}{4\pi}\alpha^3\left(\eta\times\frac{x}{|x|}\right)\sum_{j=1}^{m}\mathrm{e}^{\mathrm{i}k(\eta-x/|x|)\cdot z_j}\times\left[\left(\frac{\mu^0}{\mu^j}-1\right)\left(\mathbf{m}^j\left(\frac{\mu^0}{\mu^j}\right)\left(\eta\cdot\frac{x}{|x|}\right)+\left(\frac{\epsilon^0}{\epsilon^j}-1\right)\mathbf{m}^j\left(\frac{\epsilon^0}{\epsilon^j}\right)\right)\right]+\mathrm{O}(\alpha^4). \tag{29}$$

In the case where η and $x/|x|$ are parallel, since these two vectors are of norm 1, $x/|x|=(x/|x|\cdot\eta)\eta$. We then choose any λ non-parallel to $x/|x|$ and formula (29) becomes

$$A_\alpha\left(\frac{x}{|x|},\frac{x}{|x|},\eta,k\right)=\frac{-\mathrm{i}k^3}{4\pi}\alpha^3(\eta\times\lambda)\sum_{j=1}^{m}\mathrm{e}^{\mathrm{i}k(\eta-x/|x|)\cdot z_j}\times\left[\left(\frac{\mu^0}{\mu^j}-1\right)\left(\mathbf{m}^j\left(\frac{\mu^0}{\mu^j}\right)\left(\eta\cdot\frac{x}{|x|}\right)+\left(\frac{\epsilon^0}{\epsilon^j}-1\right)\mathbf{m}^j\left(\frac{\epsilon^0}{\epsilon^j}\right)\right)\right]+\mathrm{O}(\alpha^4). \tag{30}$$

Note that the vectors $(\eta\times x/|x|)$ in (29) and $(\eta\times\lambda)$ in (30) are known when treating the inverse problem. We have showed how formula (27) can be viewed as a special form of formula (28). That special form will provide the basis for our algorithm that reconstructs the centers z_j of the inhomogeneities.

3.1. Initial data

Based on formulas (29) and (30), the initial scalar data for the study of the recovery of the points z_j can be picked to be the following quantity:

$$g(u,v)=\sum_{j=1}^{m}\mathrm{e}^{\mathrm{i}k(v-u)\cdot z_j}\left[\left(\frac{\mu^0}{\mu^j}-1\right)\mathbf{m}^j\left(\frac{\mu^0}{\mu^j}\right)u\cdot v+\left(\frac{\epsilon^0}{\epsilon^j}-1\right)\mathbf{m}^j\left(\frac{\epsilon^0}{\epsilon^j}\right)\right], \tag{31}$$

where u and v are on the unit sphere S^2 of $\mathbf{R}^3$. The vector v is the direction of the incoming wave and the vector u the observation direction. The scalars $\mathbf{m}^j(\mu^0/\mu^j)$ and $\mathbf{m}^j(\epsilon^0/\epsilon^j)$ are given by formula (20). When solving the

inverse problem the value of g is just known for a finite set of pairs (u, v) and those values can possibly be tinted with error, but as a first step we ignore that error.

3.2. How two-dimensional algorithms can be applied to recover the z_j's

Let (z_j^1, z_j^2, z_j^3) be the coordinates of the point z_j, (u_1, u_2, u_3) and (v_1, v_2, v_3) the coordinates of u and v. In the first step we assume that $u_3 = v_3 = 0$. After applying a two-dimensional algorithm to (31) we find the pairs (z_j^1, z_j^2) for $j = 1, \ldots, m$. In the second step we assume that $u_1 = v_1 = 0$. After applying a two-dimensional algorithm to (31) we find the pairs (z_j^2, z_j^3) for $j = 1, \ldots, m$. In the third step we assume that $u_2 = v_2 = 0$. After applying a two-dimensional algorithm to (31) we find the pairs (z_j^1, z_j^3) for $j = 1, \ldots, m$. We then form classes of pairs that have same z_j^1 coordinate, classes of pairs that have same z_j^2 coordinate, and classes of pairs that have same z_j^3 coordinate. Finally, we form triplets (z_j^1, z_j^2, z_j^3), where (z_j^1, z_j^2) and (z_j^1, z_j^3) are in a class of same z_j^1 coordinate, (z_j^1, z_j^2) and (z_j^2, z_j^3) are in a class of same z_j^2 coordinate, (z_j^2, z_j^3) and (z_j^1, z_j^3) are in a class of same z_j^3 coordinate. An explicit example is provided in the following section.

3.3. The algorithm

In this section we describe our algorithm for finding (z_j^1, z_j^2) for $j = 1, \ldots, m$. The reader will understand how to use the same ideas to obtain any other subset of two coordinates from (z_j^1, z_j^2, z_j^3).

3.3.1. An intermediate quantity

We set

$$u = \begin{pmatrix} \cos\theta \\ \sin\theta \\ 0 \end{pmatrix}, \qquad v = \begin{pmatrix} \cos\phi \\ \sin\phi \\ 0 \end{pmatrix} \tag{32}$$

for two complex numbers θ and ϕ. Note that if θ and ϕ are real then our basic assumption implies that $g(u, v)$ is a measurable quantity. We want to find numerical estimates for the value of the intermediate quantity

$$\sum_{j=1}^{m} \mathrm{e}^{2\mathrm{i}(\xi_1 z_j^1 + \xi_2 z_j^2)} \left[\left(\frac{\mu^0}{\mu^j} - 1 \right) \mathbf{m}^j \left(\frac{\mu^0}{\mu^j} \right) \left(1 - \frac{2|\xi|^2}{k^2} \right) + \left(\frac{\epsilon^0}{\epsilon^j} - 1 \right) \mathbf{m}^j \left(\frac{\epsilon^0}{\epsilon^j} \right) \right] \tag{33}$$

for a vector $\xi = (\xi_1, \xi_2)$ in $\mathbf{R}^2$ in a square $[-\xi_{\max}, \xi_{\max}] \times [-\xi_{\max}, \xi_{\max}]$ and where $|\xi|$ is the usual Euclidean norm of ξ. For that purpose we need to solve for $v = (v_1, v_2)$ and $u = (u_1, u_2)$ the equation

$$v - u = \frac{2\xi}{k}, \qquad u_1^2 + u_2^2 = 1, \qquad v_1^2 + v_2^2 = 1. \tag{34}$$

Eliminating u this implies the following equation for v:

$$\xi_1 v_1 + \xi_2 v_2 = \frac{\xi_1^2 + \xi_2^2}{k}, \qquad v_1^2 + v_2^2 = 1. \tag{35}$$

Elementary algebra then shows that Eqs. (34) and (35) are always solvable if we allow u and v to be complex vectors in $\mathbf{C}^2$. In particular, if $\xi = 0$ we may choose $u = v = (1/\sqrt{2}, 1/\sqrt{2})$. Besides, supposing that k is real (k is then positive) the solutions to Eq. (34) are real if and only if $k \geq |\xi|$. This is satisfied in the square $[-\xi_{\max}, \xi_{\max}] \times [-\xi_{\max}, \xi_{\max}]$ provided that

$$k \geq \sqrt{2}\xi_{\max}. \tag{36}$$

Suppose that Eq. (34) has no real solution. This can occur if k is not real or if condition (36) is not met. Then if the imaginary parts of u and v are small enough we can still find an approximate value for $g(u, v)$ based only on values for $g(u, v)$ for u and v real and of norm 1. Here is how it works. Set

$$\tilde{g}(\theta, \phi) = g(u, v), \quad \text{where } u = \begin{pmatrix} \cos\theta \\ \sin\theta \\ 0 \end{pmatrix}, \quad v = \begin{pmatrix} \cos\phi \\ \sin\phi \\ 0 \end{pmatrix}, \tag{37}$$

$\tilde{g}$ is an entire function of (θ, ϕ) and is 2π-periodic. For θ and ϕ on the real axis, $\tilde{g}$ can be represented by its Fourier series. The convergence of that Fourier series can be extended to a band around the real axis. The convergence rate on that band is exponential. The Fourier coefficients are accurately estimated by fast Fourier transform since $\tilde{g}$ is smooth and periodic. Finally, to estimate $g(u, v)$ for u and v close to the real axis, we find complex values for θ and ϕ so as to satisfy relation (32) and we plug those values into the truncated Fourier series for $\tilde{g}$. We will show on a numerical example in a later section how that approach can be productive.

3.3.2. Utilizing the intermediate quantity

The intermediate quantity (33) can be viewed as the Fourier transform of a linear combination of Dirac measures centered at (z_j^1, z_j^2), $j = 1, \ldots, m$ and their derivatives. Therefore, a direct Fourier transform should yield the $(2z_j^1, 2z_j^2)$, $j = 1, \ldots, m$. We apply the method described in Section 1.

3.4. Numerical results

In this section we suppose that $a = 1$, that is, all the inhomogeneities that we are searching for are located in the cube $[-1, 1]^3$. In the first experiment we simulate the scattering data to be

$$\sum_{j=1}^{2} \exp(\mathrm{i}k(v-u)\cdot z_j)((0.01 + 0.03\mathrm{i})ju \cdot v - (0.3 + 2\mathrm{i})), \tag{38}$$

where $z_1 = (0.72, 0.37, 0.43)$ and $z_2 = (0.72, -0.17, -0.3)$ and $k = 21$. We choose $\xi_{\max} = 15$ so that condition (36) is satisfied, and h according to (15). With these numerical data, all solutions to Eq. (34) are real for ξ on the regular grid of the square $[-\xi_{\max}, \xi_{\max}]^2$. Then by choosing the right angles for the incoming wave and the observation point in (31), we can directly access the values of (33) for ξ on the regular grid of the square $[-\xi_{\max}, \xi_{\max}]^2$. We then apply the inverse FFT method and we plot the norm of the result for each of the planes (x, y), (y, z), (x, z) in Figs. 2.1–2.3, respectively. In Fig. 2.1, the coordinates of the two peaks are, within two decimals of accuracy, $(0.73, -0.21)$ and $(0.73, 0.31)$. In Fig. 2.2, the coordinates of the two peaks are $(-0.21, -0.32)$ and $(0.42, 0.42)$. In Fig. 2.3, the coordinates of the two peaks are $(0.73, 0.42)$ and $(0.73, -0.32)$. After matching coordinates we conclude that there must be two inhomogeneities centered at $(0.73, -0.21, -0.32)$ and $(0.73, 0.31, 0.42)$. The accuracy of this final answer agrees with the step size of the grid which is $\pi/(2\xi_{\max}) \simeq 0.105$. This numerical example illustrates how in general it is necessary to find the coordinates in all three planes (x, y), (y, z), (x, z). Indeed, had we only looked at the planes (x, y) and (x, z), we would not have been able to tell whether the final answer is $(0.73, -0.21, -0.32)$ and $(0.73, 0.31, 0.42)$ or $(0.73, -0.21, 0.42)$ and $(0.73, 0.31, -0.32)$.

In the second experiment we keep the same scattering data (38). However, this time we violate condition (36) by choosing $\xi_{\max} = 17$. Some solutions to Eq. (34) are not real. We have to interpolate the function $\tilde{g}$ defined in (37) with a truncated Fourier series. We use 64 points on $[0, 2\pi]$ for the angles θ and ϕ. The truncated Fourier series is used to calculate the intermediate quantity (33) for ξ on $[-\xi_{\max}, \xi_{\max}]^2$. We obtain slightly more accurate estimates for the location of the z_j's due to the finer grid, namely, $(0.74, 0.37)$ and $(0.74, -0.18)$ in the (x, y) plane, $(-0.18, -0.28)$ and $(0.37, 0.47)$ in the (y, z) plane, $(0.74, 0.37)$ and $(0.74, -0.28)$ in the (x, z) plane. However, we observed that the approximation of $\tilde{g}$ by a truncated Fourier series degenerates quickly as we move further away from the real axis and we could not further increase the value of $\xi_{\max}$.

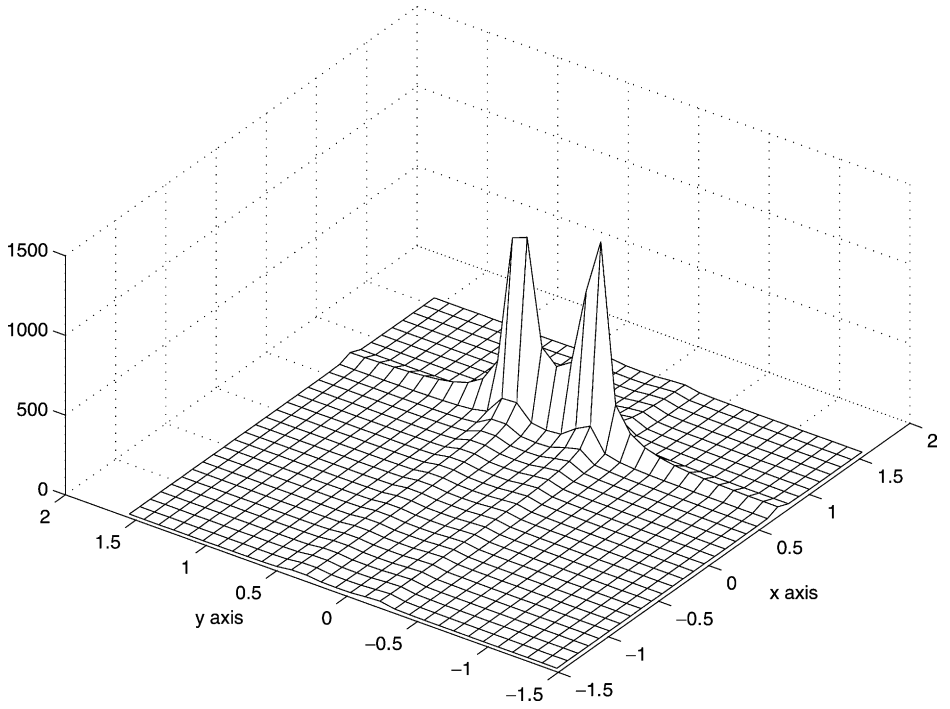

Fig. 2.1. Reconstruction in the x–y plane from the data (38).

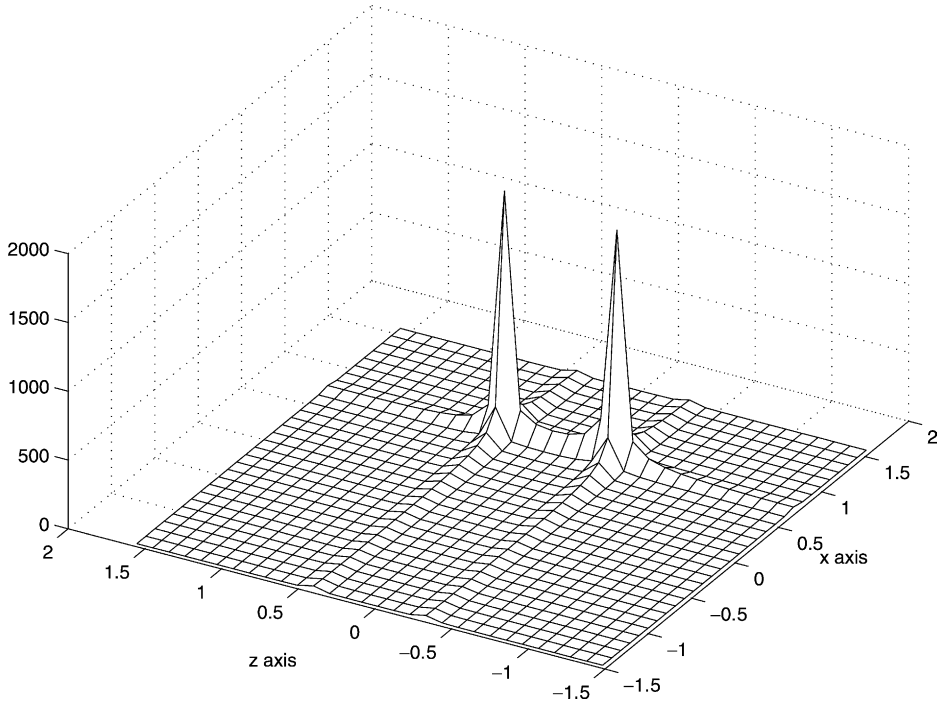

Fig. 2.2. Reconstruction in the x–z plane from the data (38).

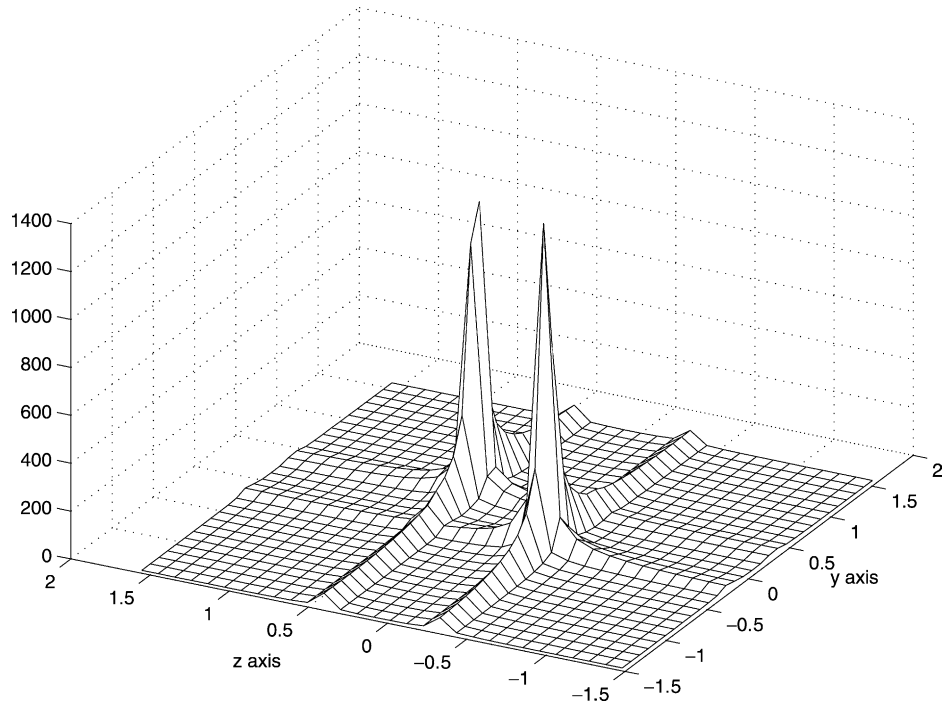

Fig. 2.3. Reconstruction in the y–z plane from the data (38).

In the third experiment we keep the same scattering data (38) but we change the value of the wavelength k into $22 + 7\mathrm{i}$. Non-real values of k model media that are conductive. We choose $\xi_{\max} = 10$. There are no real solutions to (34) so we have to represent the function $\tilde{g}$ by a truncated Fourier series. The coefficients of this series are obtained by using 64 points on $[0, 2\pi]$ for the angles θ and ϕ. We then obtain an estimate of (33) for ξ on $[-\xi_{\max}, \xi_{\max}]^2$. Numerics show that the error is acceptable, and after inverse FFT transform of the quantity (33), we derive coordinates for the z_j's, namely, $(0.79, -0.16)$ and $(0.79, 0.31)$ in the (x, y) plane, $(-0.16, -0.31)$ and $(0.31, 0.47)$ in the (y, z) plane, $(0.79, -0.31)$ and $(0.79, 0.47)$ in the (x, z) plane.

The advantage of the method that we proposed is that it does not depend on the number of inhomogeneities. That number is a priori unknown. Another advantage is that in terms of computational time this method amounts to solving three times a two-dimensional problem. A full fledged three-dimensional approach making use of spherical harmonics might be much more computationally costly.

To illustrate the fact that our method does not depend on the number of inhomogeneities, we present another example where we have seven points z_j whose coordinates are given in the following table:

	x coordinate	y coordinate	z coordinate
z_1	0.72	0.37	0.43
z_2	0.72	−0.17	−0.3
z_3	0.72	−0.17	0.43
z_4	−0.52	−0.17	−0.3
z_5	−0.9	0.0	0.0
z_6	0.0	−0.5	−0.0
z_7	0.0	0.37	0.43

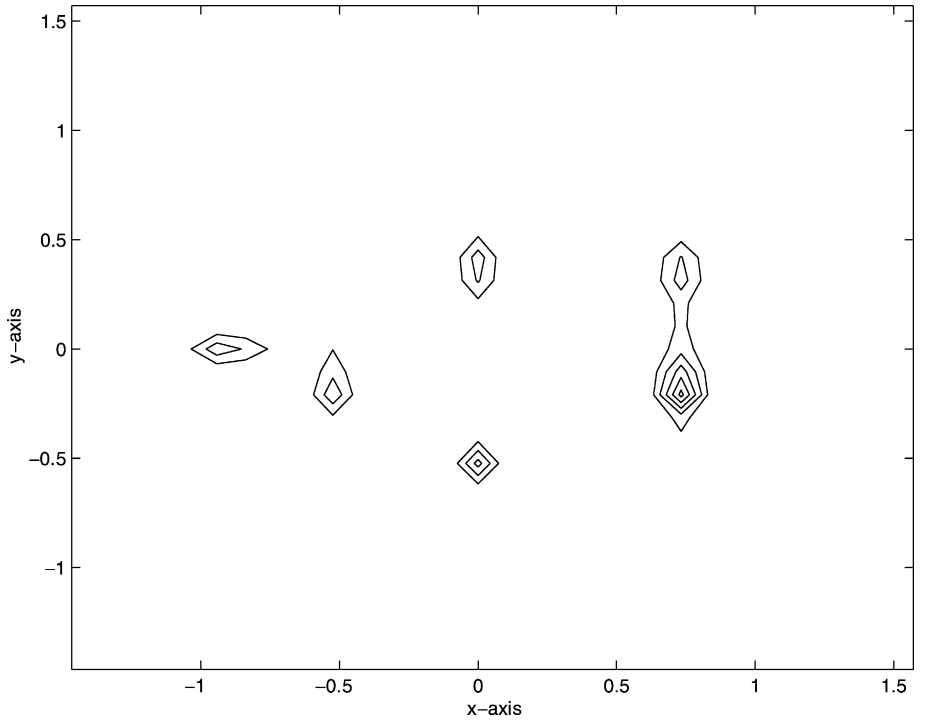

Fig. 2.4. Reconstruction in the x–y plane from the data (39).

We still assume that $a = 1$ and that the scattered far field pattern is

$$\sum_{j=1} \exp(\mathrm{i}k(v-u)\cdot z_j)\left((0.01+0.03\mathrm{i})\frac{j}{3}u\cdot v-(0.3+2\mathrm{i})\right), \tag{39}$$

where the value for the wavelength k is 22. In this case, just as in the first experiment, we choose $\xi_{\max} = 15$ and all solutions to Eq. (34) are real. We then apply the inverse FFT method and we plot contour lines for the norm of the result for each of the planes (x, y), (y, z), (x, z) in Figs. 2.4–2.6, respectively. The step size for the grid is again $\pi/(2\xi_{\max}) \simeq 0.105$. In Fig. 2.4 we observe six peaks located at

$$A_1 = (-0.94, 0.0), \quad A_2 = (-0.52, -0.21), \quad A_3 = (0.0, -0.52),$$
$$A_4 = (0.0, 0.42), \quad A_5 = (0.73, -0.21), \quad A_6 = (0.73, 0.31).$$

In Fig. 2.5 we observe five peaks located at

$$B_1 = (-0.52, 0.0), \quad B_2 = (-0.21, -0.31), \quad B_3 = (-0.21, 0.42),$$
$$B_4 = (0.0, 0.0), \quad B_5 = (0.42, 0.42).$$

In Fig. 2.6 we observe six peaks located at

$$C_1 = (-0.94, 0.0), \quad C_2 = (-0.52, -0.31), \quad C_3 = (0.0, 0.0),$$
$$C_4 = (0.0, 0.42), \quad C_5 = (0.73, -0.31), \quad C_6 = (0.73, 0.42).$$

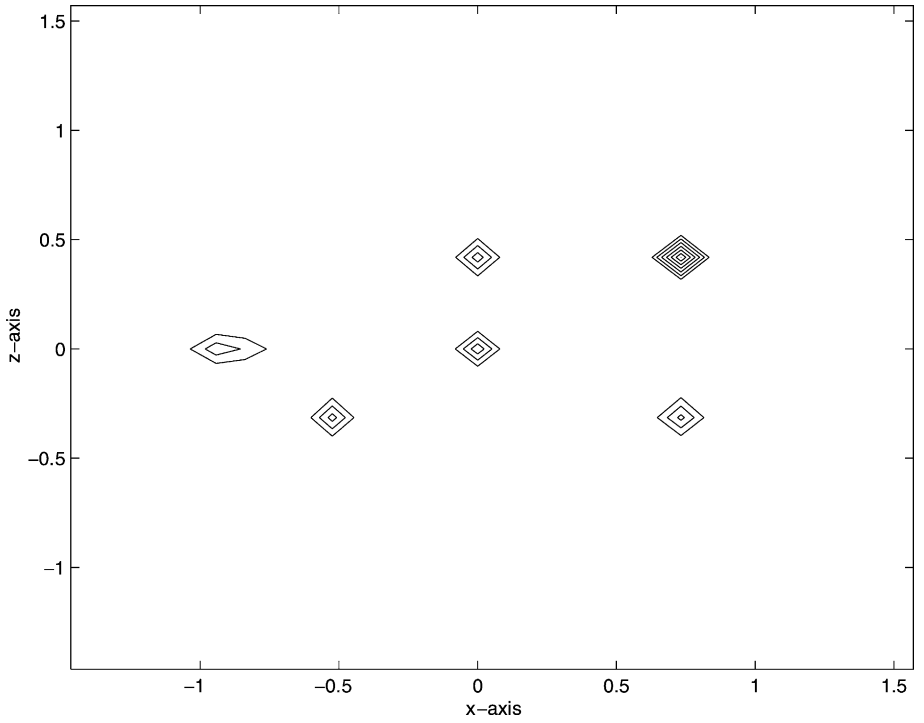

Fig. 2.5. Reconstruction in the x–z plane from the data (39).

We then put in the same class the points A_j and B_l that have the same y coordinate or whose y coordinates differ from no more than one step size. The classes are

$$\{A_1, B_4\}, \qquad \{A_2, A_5, B_2, B_3\}, \qquad \{A_3, B_1\}, \qquad \{A_4, A_6, B_5\}.$$

Next we put in the same class the points A_j and C_l that have the same x coordinate or whose x coordinates differ from not more than one step size. The classes are

$$\{A_1, C_1\}, \qquad \{A_2, C_2\}, \qquad \{A_3, A_4, C_3, C_4\}, \qquad \{A_5, A_6, C_5, C_6\}.$$

Next we put in the same class the points B_j and C_l that have the same z coordinate or whose z coordinates differ from not more than one step size. The classes are

$$\{B_1, B_4, C_1, C_3\}, \qquad \{B_2, C_2, C_5\}, \qquad \{B_3, B_5, C_4, C_6\}.$$

We are now ready to find the approximate coordinates for the centers of the inhomogeneities. It suffices to arrange triplets (A_j, B_l, C_m) such that the pairs A_j and B_l, A_j and C_m, B_l and C_m are in one of the classes listed above. We find seven such triplets

$$(A_1, B_4, C_1), \qquad (A_2, B_2, C_2), \qquad (A_3, B_1, C_3), \qquad (A_4, B_5, C_4),$$
$$(A_6, B_5, C_6), \qquad (A_5, B_2, C_5), \qquad (A_5, B_3, C_6).$$

These triplets correspond to the points in the (x, y, z) plane

$$(-0.94, 0.0, 0.0), \qquad (-0.52, -0.21, -0.31), \qquad (0.0, -0.52, 0.0), \qquad (0.0, 0.42, 0.42),$$
$$(0.73, 0.31, 0.42), \qquad (0.73, -0.21, -0.31), \qquad (0.73, -0.21, 0.42).$$

We were able to recover the coordinate points z_j's within the announced accuracy.

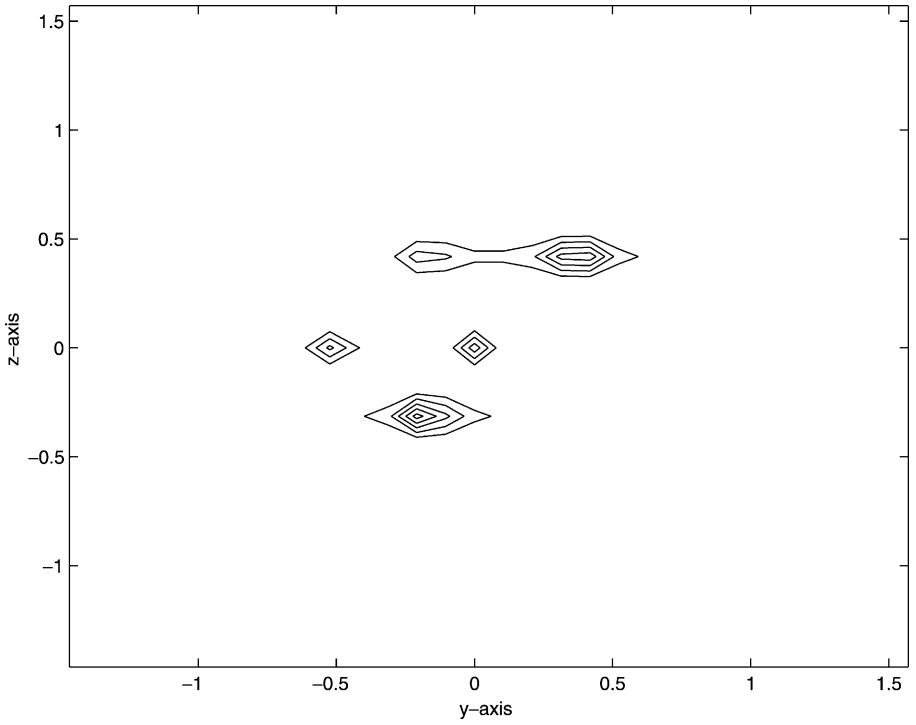

Fig. 2.6. Reconstruction in the y–z plane from the data (39).

Acknowledgements

The author would like to thank Shari Moskow from the University of Florida for the enriching discussions they had about this work and for her encouragements.

References

[1] H. Ammari, E. Lakovleva, S. Moskow, Recovery of small inhomogeneities from the scattering amplitude at a fixed frequency, SIAM J. Math. Anal., submitted for publication.
[2] H. Ammari, S. Moskow, M.S. Vogelius, Boundary integral formulae for the reconstruction of electric and electromagnetic inhomogeneities of small volume, ESAIM: Cont. Opt. Calc. Var. 9 (2003) 49–66.
[3] H. Ammari, J.K. Seo, An accurate formula for the reconstruction of conductivity inhomogeneities, Adv. Appl. Math., in press.
[4] H. Ammari, A. Khelifi, Electromagnetic scattering by small inhomogeneities, in press.
[5] H. Ammari, D. Polkas, The leading order term in the asymptotic expansion of the scattering amplitude of a collection of finite number of dielectric inhomogeneities of small diameter, Math. Meth. Appl. Sci., in press.
[6] H. Ammari, D. Volkov, Correction of order three for the expansion of two-dimensional electromagnetic fields perturbed by the presence of inhomogeneities of small diameter, in press.
[7] H. Ammari, M.S. Vogelius, D. Volkov, Asymptotic formulas for perturbations in the electromagnetic fields due to the presence of inhomogeneities of small diameter. II. The full Maxwell equations, J. Math. Pure Appl. 80 (8) (2001) 769–814.
[8] J. Blitz, Electrical and Magnetic Methods of Nondestructive Testing, IOP Publishing, Adam Hilger, New York, 1991.
[9] D.L. Colton, R. Kress, Inverse acoustic and electromagnetic scattering theory, in: Applied Mathematical Science, vol. 93, Springer, New York, 1992.
[10] D.J. Cedio-Fengya, S. Moskow, M.S. Vogelius, Identification of conductivity imperfections of small diameter by boundary measurements. Continuous dependence and computational reconstruction, Inv. Probl. 14 (3) (1998) 553–595.

[11] A. Friedman, M.S. Vogelius, Identification of small inhomogeneities of extreme conductivity by boundary measurements: a theorem on continuous dependence, Arch. Rat. Mech. Anal. 105 (1989) 299–326.
[12] R. Kress, Linear integral equations, in: Applied Mathematical Sciences, vol. 82, 2nd ed., Springer, New York, 1999.
[13] P. Maponi, L. Misici, F. Zirilli, An inverse problem for the three-dimensional vector Helmholtz equation for a perfectly conducting obstacle. Multidimensional inverse problems, Comput. Math. Appl. 22 (4–5) (1991) 137–146.
[14] A.B. Movchan, S.K. Serkov, The Pólya–Szegö matrices in asymptotic models of dilute media, Eur. J. Appl. Math. 8 (1997) 595–621.
[15] J.C. Nédélec, Acoustic and electromagnetic equations. Integral representations for harmonic problems, in: Applied Mathematical Sciences, vol. 144, Springer, New York, 2001.
[16] G. Pólya, G. Szegö, Isoperimetric inequalities in mathematical physics, in: Annals of Mathematical Studies, vol. 27, Princeton University Press, Princeton, NJ, 1951.
[17] M. Schiffer, G. Szegö, Virtual mass and polarization, Trans. AMS 67 (1949) 130–205.
[18] M.S. Vogelius, D. Volkov, Asymptotic formulas for perturbations in the electromagnetic fields due to the presence of inhomogeneities of small diameter, M2AN Math. Model. Numer. Anal. 34 (4) (2000) 723–748.
[19] D. Volkov, An inverse problem for the time harmonic Maxwell's equations, Ph.D. Thesis, Rutgers, New Brunswick, NJ, 2001.